

# Thermal Instability and Magnetic Pressure in the Turbulent Interstellar Medium

Enrique Vázquez-Semadeni<sup>1</sup>, Adriana Gazol<sup>1</sup>, Thierry Passot<sup>2</sup>, and Javier Sánchez-Salcedo<sup>3</sup>

<sup>1</sup> Instituto de Astronomía, UNAM, Campus Morelia, Apdo. Postal 3-72, Morelia, Michoacán, MEXICO

<sup>2</sup> CNRS, Observatoire de la Côte d’azur, B.P. 4229, 06304, Nice, Cédex 4, France

<sup>3</sup> Instituto de Astronomía, UNAM, Apdo. Postal 70-264, México, D.F., 04510, México

**Abstract.** We review recent results on the nonlinear development of thermal instability (TI) under the isobaric criterion, in the context of the turbulent atomic interstellar medium (ISM), in which density and velocity fluctuations are present, as well as forces other than the thermal pressure gradient. First, we discuss the growth of entropy perturbations in isolation, as a function of the ratio of the cooling time to the dynamical crossing time  $\eta$ . We verify that, for  $\eta \ll 1$ , isobaric initial perturbations do not proceed isobarically, but instead develop large transient pressure gradients that cause the condensation process to be highly dynamical, with supersonic inflow motions, and with the formation of an outwards-propagating shock that brings the surrounding medium out of thermal equilibrium. In our simulations, the time for the dynamical transient state to subside ranges from 4 to 30 Myr for initial density perturbations of 20% and sizes 3 to 75 pc. By the time the condensations have formed, a substantial fraction of the mass is still traversing the unstable range. Second, we consider the evolution of *velocity* perturbations, maintained by a random forcing. We numerically find that the growth of fluctuations can be suppressed for arbitrarily long times if the forcing causes a moderate rms Mach number ( $\gtrsim 0.3$ ), with an increase in the total internal energy greater than a factor of 2, and extends to small enough scales or occurs in low enough density environments that  $\eta > 1$  at those scales. From the two sets of results, we conclude that, even if TI were the sole cloud-forming agent in the ISM, static, thermal pressure-confined clouds are unlikely to exist in the ISM.

We then consider the behavior of magnetic pressure in turbulent regimes. We confirm earlier results that the magnetic pressure does not correlate well with density at low and intermediate densities, and propose that this is a consequence of the different scaling of the magnetic field strength with density for the slow and fast modes of nonlinear MHD waves. We remark that this lack of correlation implies that magnetic “pressure” is not a suitable candidate for supplementing thermal pressure in the presence of TI, and that polytropic descriptions of it are probably not adequate in the fully turbulent regime. Finally, we discuss the role of TI in a turbulent ISM-like medium. It is found that the medium does not exhibit sharp phase transitions, as would be expected in classical multiphase models of the ISM, and instead a continuum of density and temperature is found in numerical simulations, in which a substantial fraction of the mass is again in the unstable range. This appears to be a result of the internal energy injection from the forcing and of the continuous transit of gas through the phases, rather than of the pressure supplied by the magnetic field.

## 1 Introduction

The fact that the neutral atomic interstellar medium (ISM) is most likely thermally bistable [16,56] has had a great impact on our picture of interstellar structure formation. Indeed, in two of the most influential models of the ISM to date, the famous two- and three-phase models of the ISM [16,38], the concepts of thermal and pressure equilibria played a fundamental role, so that distinct *phases* (thermodynamic regimes with different density and temperature, but the same pressure) were predicted to coexist in pressure equilibrium. These phases correspond to stable thermal-equilibrium (heating-cooling balance) temperature regimes, and are separated by unstable regimes that, in those models, were therefore not expected to be present in the ISM. An opposite view was taken in the so-called time-dependent model of the ISM [19], which was presented as an alternative to the pressure equilibrium two-phase model, and which made radically different assumptions: a constant density in the presence of stochastic, local heating events that caused strong local fluctuations of pressure and temperature, because the cooling and recombination times are comparable or shorter than the time between exposure of a given gas parcel to one of those heating events. This model predicted that significant amounts of gas should be in the unstable range, as they cooled after the transient heating events. More recently, reference [34] has considered a continuous recycling of gas among the various gas phases, also concluding that significant amounts of gas should populate the unstable temperature range in the ISM. Note that the three-phase model [38] did consider the existence of local fluctuations in the pressure, although it was still based on the premise of “rough pressure balance”.

Nevertheless, both the equilibrium and the time dependent models omitted a number of important aspects in the ISM budget. The multiphase equilibrium models essentially neglected the possibility of large pressure fluctuations in the ISM. The time dependent model instead included this possibility as a fundamental premise, but still neglected the fact that such fluctuations should induce motions, which should in general be turbulent and cause strong density fluctuations. The turbulence involves gas motions at all scales which not only provide ram “pressure”, but also mixing, and can produce compressions rather than “support” [13,2]. In fact, turbulent motions alone can account for the cloud/intercloud structure of the ISM even without TI-inducing cooling functions [46]. Moreover, both the time-dependent and the three-phase models omitted other important agents of the ISM, such as magnetic fields, rotation, and cosmic rays. References [11,14] performed a combined instability analysis including self-gravity, cooling and heating, and magnetic fields, but the effects of turbulence, which is an inherently nonlinear phenomenon, can only be dealt with by means of numerical simulations of the gas dynamics in the Galactic disk in the presence of TI.

Several workers have studied the nonlinear development of the thermal instability (TI), though mainly in the context of the formation of proto-galactic and proto-globular cluster cloud formation (e.g., [9,40,41,27]). In the context of the ISM, recent work has investigated the triggering of TI by external compressions ([22,23,30]) and the fragmentation of clouds into clumps [6]. However, the

possibility raised by [9] in the context of galactic cooling flows that supersonic motions should develop during the condensation process, and its consequences on the likelihood of the existence of thermal-pressure bounded clouds in the ISM, had not been discussed until recently. References [55,31,32] have suggested that the interstellar turbulence may be powered by the development of TI. Thus, it is important to quantify the conditions under which the condensation<sup>1</sup> process is dynamic, the magnitude of the velocities developed, and the duration of the dynamic stage.

Moreover, several observational studies (e.g., [10,21]) have suggested that the fraction of gas in the unstable range between the cold and warm phases of the atomic ISM is substantial. It is reasonable to assume that this may be a consequence of the presence of (MHD) turbulence in the unstable medium. Thus, it is important to investigate the development of TI in the presence of velocity fluctuations and the possible role of the magnetic field in supplying additional pressure to compensate the “inverse” thermal-pressure regime that occurs under the isobaric mode of TI.

In this paper, we summarize recent work in these areas by references [49] (hereafter Paper I), [47] (hereafter Paper II), [18] (hereafter Paper III), and [54] (hereafter Paper IV)<sup>2</sup>, and attempting to present it in a comprehensive, coherent fashion. Papers I, III and IV concern gas unstable under the *isobaric* mode of TI (relevant to the transition between the warm and cold phases of the ISM), while Paper II concerns the nature of magnetic pressure in isothermal turbulent media. First, we present the numerical model in §2 and a qualitative discussion of the instability in §3. Then, in §4, we discuss the degree to which the condensation process can give rise to large (transonic) velocities, and how long do these motions last, as a function of the ratio of the cooling to sound crossing times, hereafter denoted  $\eta$ . Next we discuss the evolution of velocity perturbations, rather than the isobaric density perturbations normally considered in studies of the isobaric mode of TI (§5), stressing that these constitute the most realistic way of inducing density fluctuations in turbulent media. We then briefly discuss the nature of magnetic pressure on turbulent media (§6). Afterwards, motivated by observational work that has claimed to find significant amounts of HI gas in the unstable range between the cold and warm phases [10,26,52,17,21], we discuss the role of TI in numerical models of the ISM in the presence of magnetic fields, the Coriolis force, modeled star formation, self-gravity and TI, aiming at determining the fraction of unstable gas, and at interpreting the results in the light of the previous sections (§7). Finally, we present some conclusions in §8.

---

<sup>1</sup> For consistency with the nomenclature in the literature, we maintain the name “condensation” even for highly dynamic cases in which “accretion” or “collapse” might be more appropriate.

<sup>2</sup> This order reflects the logical sequence of the papers rather than the chronological one.

## 2 The models

In the work summarized here, various different setups have been considered. Paper I considered the case of pure hydrodynamical flows in one dimension (1D) in the presence of cooling and background heating terms that model the corresponding radiative processes in the atomic ISM (see below), and with the possible inclusion of a random forcing process. Paper III first considered a similar setup in two dimensions (2D) and then added the magnetic field, the Coriolis force, and a sinusoidal shear (a crude representation of the Galactic shear due to the differential rotation), and substituted the random forcing for a stellar-like one, with local sources of heat, which turn on when the local density exceeds a certain threshold, and stay on for 6 Myr. The latter setup was also used in Paper IV, except with a slightly modified cooling function. Paper II, on the other hand, considered isothermal MHD flows with random forcing in “1+2/3 D”, or slab geometry, meaning that all three components of vector quantities are solved for, but spatial derivatives are considered only along one spatial dimension. In all cases, the ideal gas equation of state,  $P = (\gamma - 1)c_v\rho T$ , is assumed, where  $\gamma = 5/3$  is the heat capacity ratio  $c_p/c_v$  for monoatomic gases. The numerical scheme used in Paper I was a sixth-order finite difference one, described in [48], while Papers II, III and IV used a pseudospectral scheme, using hyperviscosity in the latter two.

In all cases with heating and cooling, the internal energy equation is written per unit mass, and we have used simplified forms for those functions, consisting of simple piecewise-power law fits to standard cooling functions, and a constant background heating. Papers I and IV used a fit to the “standard” cooling function of [56], while Paper III used slight modifications to the fit of [7] to the cooling functions of [8], since the original fits of [7] do not cause any unstable temperature range. The piecewise power law fits had the form

$$A = C_{i,i+1}T^{\beta_{i,i+1}} \quad \text{for } T_i \leq T < T_{i+1}, \quad (1)$$

## 3 Review of TI and the role of the ratio of cooling time to crossing time

The full linear analysis leading to TI was first performed in the classic paper of Field [15], and later generalized by references [24,25] to the case of a flow in motion. More recent useful discussions may be found in [12,51]. The linear analysis is known to yield a cubic dispersion relation, having one root that is always real and a pair that may be complex or real. Real roots correspond to the so-called *condensation* (or thermal) mode, while complex roots correspond to the so-called *wave* mode. The modes are unstable when the real (parts of the) roots are positive.

A key parameter for many of the issues discussed in this paper is the ratio  $\eta$  of the cooling time  $\tau_c$  to dynamical time  $\tau_d$ . This ratio is inversely proportional to the product of the wavelength of the perturbation and the equilibrium cooling

rate. In this paper we often consider this parameter rather than a normalized length scale (or wave number, as in [15]) because this allows us to consider cases of perturbations with the same physical size (in pc), even if they correspond to different values of  $\eta$  due to, say, differences on the equilibrium cooling rate (or, equivalently, the background density).

It is well known (e.g., [15,51]) that for initial perturbations in entropy<sup>3</sup> of vanishing wavelength ( $\eta \gg 1$ , with the dynamical time here being given by the sound crossing time  $\tau_s$ ), the condensation mode evolves isobarically, and is then called the *isobaric* mode. In the opposite limit of very large wavelengths, it behaves isochorically, being then called the *isochoric* mode. Each mode has its own corresponding instability criterion, and, in our case of a constant background heating function and a cooling given by (1), the isobaric and isochoric criteria are respectively  $\beta_{ij} < 1$  and  $\beta_{ij} < 0$ . In general, the growth rates increase with decreasing wavelength (or  $\eta$  increases), approaching a maximum constant rate (the inverse of the cooling time – see below) in the zero-conductivity case, or reaching a maximum and then decreasing again, until finally becoming zero at the so-called Field length in the thermally conducting case [15,3])

Entropy perturbations with  $\eta > 1$  evolve almost quasi-statically, maintaining quasi-isobaricity throughout their evolution. On the other hand, entropy perturbations with  $\eta < 1$  cool before they can equate pressures and therefore develop large pressure gradients, which then cause them to evolve highly dynamically even if only the isobaric instability criterion is satisfied [15,1,39]. In the latter case, the growth rate approaches zero in the limit of large wavelengths, while in order for finite growth rates to exist in this limit, it is necessary to also satisfy the isochoric criterion. In fact, perturbations with  $\eta > 1$  grow on time scales  $\sim \tau_c$ , because in this case the perturbation can only evolve as fast as it cools. Instead, perturbations with  $\eta < 1$  grow on a time  $\sim \tau_s$ , because they can only evolve as fast as the pressure gradient pushes the gas surrounding the condensation to equate pressures. These two time scales constitute the limits of the zero-conductivity curve in fig. 2 of reference [15]. This implies that, when only the isobaric criterion is satisfied, the thermal evolution leads back to thermal equilibrium, while the dynamic evolution undergoes runaway growth. On the other hand, when the isochoric criterion is also satisfied, the thermal evolution also runs away from thermal equilibrium.

The case of wavelike (or “adiabatic”) perturbations is perhaps the most relevant for a turbulent ISM since, in this case, the adiabaticity condition implies that a compressive or expansive motion was required in order to produce a density fluctuation accompanied by a pressure fluctuation of the same sign. That is, this is the type of perturbations produced by *velocity* fluctuations which, we stress, *are the only realistic way of producing a density fluctuation in an initially*

<sup>3</sup> Recall that, for reversible processes, adiabatic processes are isentropic, and are characterized by keeping the ratio  $P/\rho^\gamma$  constant. Thus, entropy perturbations are those which change this ratio, such as, for example, isobaric density fluctuations.

*uniform medium*<sup>4</sup>, because the gas is subject to the continuity equation (mass conservation), so that a density enhancement requires a converging velocity field. This kind of perturbations becomes unstable when the adiabatic instability criterion is satisfied. For our cooling function, this requires  $\beta_{ij} < 1/(1-\gamma) = -3/2$ .

In the presence of velocity fluctuations, the dynamical time  $\tau_d$  to use in  $\eta$  should be chosen as the minimum of the sound and the bulk velocity crossing times, respectively denoted  $\tau_s$  and  $\tau_u$ . The wavelike perturbations are known [15,51] to evolve as quasi-adiabatic (possibly overstable, i.e., of growing amplitude) sound waves (corresponding to a complex conjugate pair of roots of the dispersion relation) for  $\eta \gg 1$ , while for  $\eta \ll 1$  they evolve as “effective” sound waves with a propagation speed that is given by

$$c_{\text{eff}} = \left[ \frac{1}{\gamma} \frac{(\partial \mathcal{L} / \partial T)_P}{(\partial \mathcal{L} / \partial T)_\rho} \right]^{1/2}, \quad (2)$$

where  $\mathcal{L}$  is the net cooling minus heating function and  $\gamma$  is heat capacity ratio. Thus, the response of the flow to velocity fluctuations ranges between thermal-equilibrium and adiabatic as  $\eta$  is varied from  $\ll 1$  to  $\gg 1$ , while entropy perturbations can only range between thermal-equilibrium and isobaric. This is because *in the case of velocity (wavelike) perturbations, the velocity field (initially) drives the pressure gradient*, while the opposite happens for entropy perturbations.

In the limit  $\eta \ll 1$ , if the isobaric instability criterion is satisfied (but not the isochoric nor the adiabatic ones), the effective sound speed becomes imaginary, and the “waves” do not propagate nor evolve adiabatically, but instead become a condensation mode, in a similar way as to what happens to isobaric entropy perturbations in this same limit, which do not evolve isobarically.

In the particular case of a (piecewise) power-law cooling function (1) and constant background heating, the limit  $\eta \ll 1$  implies that the pressure approaches the thermal-equilibrium value given by  $P_{\text{eq}} \propto \rho^{\gamma_{\text{eff}}}$ , where  $\gamma_{\text{eff}} = (\beta_{ij} - 1)/\beta_{ij}$ . We refer to this behavior as a (piecewise) effective polytropic behavior [53]. Also in this limit, the effective sound speed of the wave mode is given by  $[(\beta_{ij} - 1)/\beta_{ij}]^{1/2}$ . The wave ceases to propagate when  $(\beta_{ij} - 1)/\beta_{ij} < 0$ , i.e., when  $0 < \beta_{ij} < 1$ , so that the isobaric criterion is satisfied.

The equilibrium pressure  $P_{\text{eq}}$  for the cooling function fits used in Papers I and IV is shown in fig. 1. In this figure, we denote by  $\rho_{\text{isob}}$  the density value within the cold phase that corresponds to the equilibrium pressure at the mean density. The behavior of  $P_{\text{eq}}$  shown in fig. 1 implies that the range  $300 \lesssim T \lesssim 6000$  K (equivalent to the density range  $0.6 \text{ cm}^{-3} \lesssim \rho \lesssim 3.2 \text{ cm}^{-3}$  in thermal equilibrium) is (only) isobarically unstable, with  $\beta_{ij} \sim 1/2$ . This corresponds to the unstable range between the so-called cold and warm phases of the atomic ISM. Note also the  $\gamma_{\text{eff}} = 0$  behavior in the range  $3.2 \text{ cm}^{-3} \lesssim \rho \lesssim 7.1 \text{ cm}^{-3}$ . A similar (though not identical)  $P_{\text{eq}}$  curve was used in the unstable cases considered in Paper III.

---

<sup>4</sup> Real-world entropy fluctuations could only be produced by locally varying the cooling-to-heating ratio.

## 4 Dynamics of the condensation mode

In this section we discuss the conditions necessary for the development of large velocities (possibly supersonic) and shocks during the condensation process of an *entropy* perturbation that is unstable with respect to the isobaric condition in the atomic ISM, as a function of the parameter  $\eta$ . We are also interested in the duration of the dynamic phase. Studies dealing with the development of supersonic motions and shocks during the condensation process have generally considered the regime of proto-galactic and proto-globular cluster clouds (e.g., [9,5,27]. A detailed discussion of the nature of the shocks has been presented in [39]. However, here we are interested in this problem in the context of the atomic ISM, so that then we can discuss the likely state of clouds formed by TI in the ISM and whether gas in the unstable range is to be expected. We follow the discussion of Paper I closely.

We first consider the case of small-scale (actually,  $\eta \sim 1$ ) entropy perturbations, as they constitute the paradigm of cloudlet (i.e., small clouds of sizes  $\lesssim 1$  pc and densities  $\sim 50 \text{ cm}^{-3}$ ) formation by TI in the ISM (e.g., [50,45,34]). To this end, we have performed a 1D simulation, labeled DEN3, of the evolution of a Gaussian density perturbation of 20% amplitude and a full width at half maximum (FWHM) of 3 pc over a mean density of  $1 \text{ cm}^{-3}$ , roughly the volume average density of the Galactic ISM. We start the simulation at  $T \sim 2500$

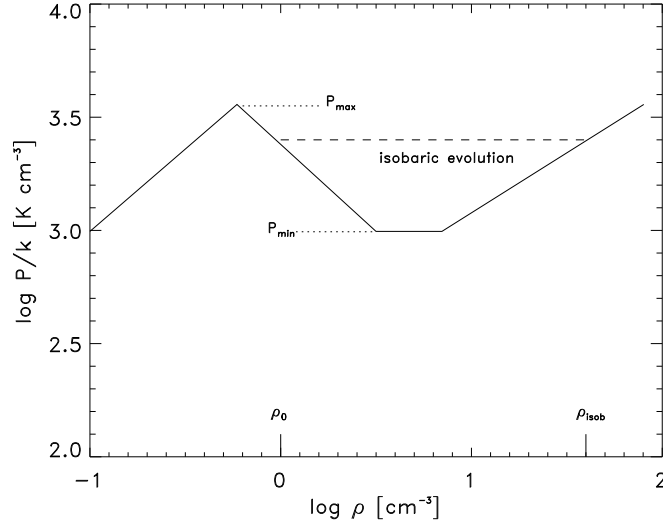


**Fig. 1.** Thermal-equilibrium piecewise polytropic behavior of the pressure for the cooling functions used in Papers I and IV.  $\rho_{\text{isob}}$  is the value of the density within the cold phase whose corresponding thermal-equilibrium pressure equals that of the mean density  $\rho_0$ .

$K$ , the thermal-equilibrium temperature at the mean density. Note that these conditions lie in the unstable range. Figure 2 shows the density, pressure and velocity profiles of the cloud at various times until the time when a “cloud” has formed and the accretion process has mostly subsided. Note the logarithmic  $x$ -axis, where  $x$  is the distance to the center of the cloud. It is seen that the evolution is indeed quasi-isobaric, with variations in the pressure of less than 2%, and local Mach numbers which do not exceed 0.2. By  $t = 4.2$  Myr, the condensation has essentially completed its evolution, and reached the pressure-equilibrium density,  $\rho_{\text{isob}}$ . Figure 3 shows the evolution of this run on the  $P$ - $\rho$  diagram. The quasi-isobaric nature of the condensation is clearly seen, especially at the final time, at which all points with densities higher than the mean have almost exactly the same pressure.

Note, however, that in fig. 2 a population of points is still seen to continue flowing onto the condensation, and as it does, it necessarily remains in the unstable range. In fact, the mass of this gas amounts to  $\sim 8$  times the mass in the condensation. In fig. 2, it is seen that this occurs in the region  $0 \gtrsim \log |x|/\text{pc} \gtrsim -1.5$ . The accretion and evacuation of the unstable gas will take very long times to complete, because the reservoir of unstable gas outside the cloud is very large ( $\sim 90\%$  of the total mass). Moreover, note that the inflowing gas is not truly unstable, as it does not lie on the equilibrium curve anymore. Instead, at  $t = 4.2$  Myr, the density and pressure gradients have the same sign throughout this region. Thus this gas does not have a tendency to fragment any further, even though its density is in the “unstable” range. Finally, note that the

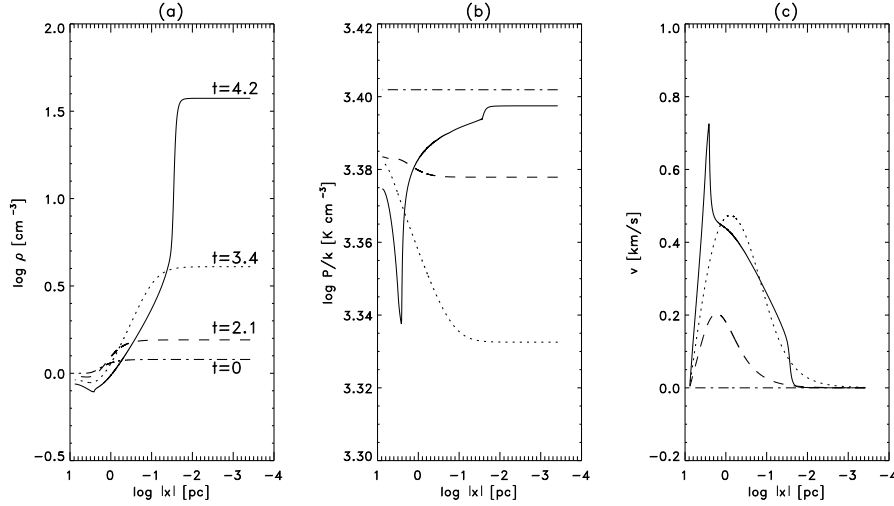


**Fig. 2.** Time development of run DEN3. The density, pressure and velocity profiles at different times are plotted in panels (a), (b) and (c), respectively. The times corresponding to each line type are indicated in frame (a) in Myr, and the same line labeling is used in frames (b) and (c).



cloud formation time is not very short, and is significantly sensitive to the initial amplitude. Simulations with an initial amplitude of 10% require  $\sim 5.5$  Myr to complete the condensation. This time is comparable to the mean time between successive exposures to passing shock fronts from supernova remnants and superbubbles [28], so that the condensations may have their growth interrupted by external perturbations, as is the case in §5.

Let us now consider the opposite case of a large-scale entropy perturbation, with FWHM=75 pc and  $\eta \sim 0.04$ , in a box of 250 pc. We refer to this simulation as run DEN75. Its evolution is shown in figs. 4 (density, pressure and velocity profiles) and 5 (evolution on the  $P$ - $\rho$  plane). In this case, the evolution is significantly different. As dictated by the smaller growth rates of larger-scale perturbations, run DEN75 requires 30 Myr to complete the formation of a cloud, but moreover, throughout the first part of its development, the condensation proceeds along the thermal equilibrium curve (see the first four panels of fig. 5), developing supersonic velocities in the process (maximum Mach number  $\sim 1.2$ ) that cause a strong overshoot. Thus, this condensation transiently reaches densities  $\sim 55\rho_{\text{isob}}$ . At the time of maximum compression, a strong shock is produced at the cloud boundary that propagates outwards from it. This shock weakens quickly as it propagates into the low density medium, but it has the important effect of throwing the still infalling gas off thermal equilibrium, restoring near pressure balance (last two panels of fig. 5) and strongly reducing the accretion speed. By the end of the simulation, however, the accretion ram pressure is still high enough that the condensation has  $\rho \sim 3\rho_{\text{isob}}$ , and this value decreases extremely slowly with time. Again, as in run DEN3, the infalling gas is mostly in the “unstable” density range, in this case with a mass of almost twice that in the cloud. Within the infalling region, the pressure and density gradients have the same sign, so this gas again has no further tendency to fragment. We have

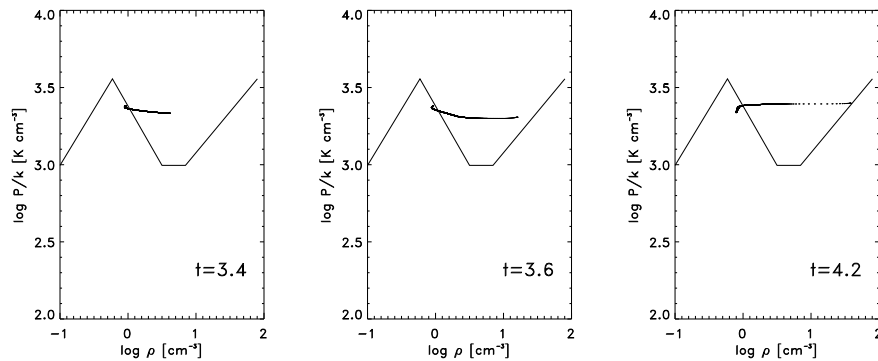


**Fig. 3.** Time development of run DEN3 in  $P$ - $\rho$  phase space, at the times indicated in each frame. At  $t = 4.2$  Myr, although the cloud has already formed, a substantial fraction of the points in the simulation are still traversing the unstable range, albeit in a nearly isobaric regime.

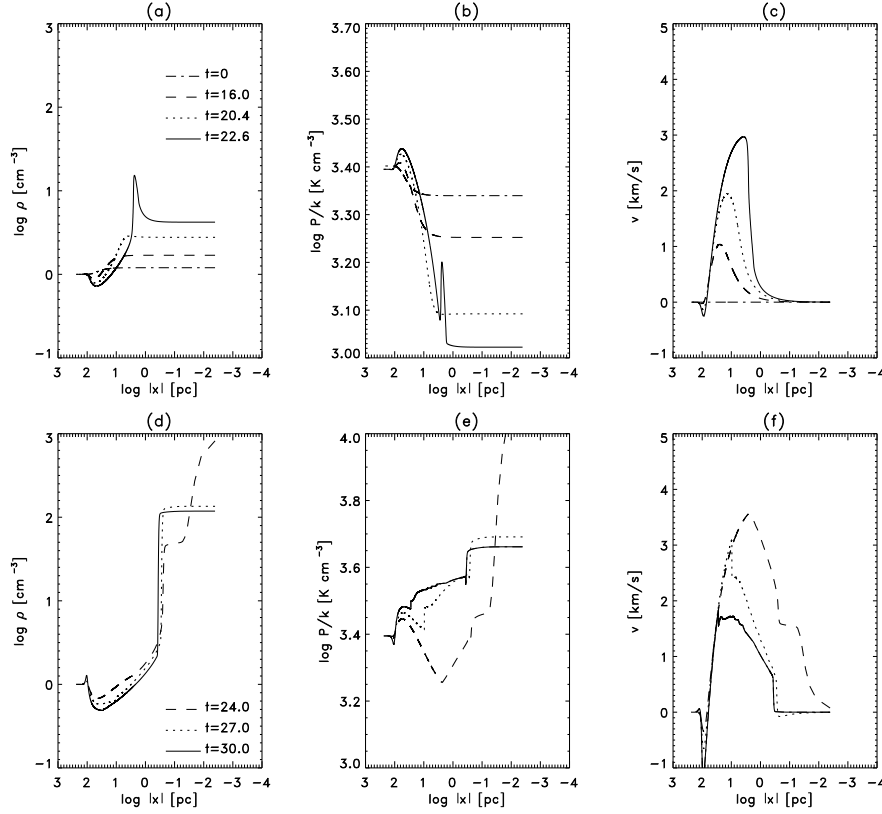


**Fig. 4.** Same as fig. 2 but for run DEN75. The first part of the evolution is shown in the upper frames, and the rest in the lower frames. Note the formation of a shock shortly after  $t = 22.6$  (frame c), which then propagates outwards from the cloud. At the same time, the density overshoots to over  $55\rho_{\text{isob}}$  (frame d). After the formation of the cloud, the density relaxes to a value  $\sim 3\rho_{\text{isob}}$ , due to the ram pressure of the still infalling gas.

found from other simulations that the qualitative behavior of run DEN75 occurs down to initial fluctuations with  $\text{FWHM}=15$  pc.

From the evolution of these two simulations, we conclude that large-scale ( $\eta \ll 1$ ) entropy perturbations have such a dynamic evolution that their final density does not correspond to pure thermal-pressure equilibrium, and moreover require such long times to evolve (over 20 Myr to the occurrence of the large density transient), that they are unlikely to complete their evolution before being disrupted by other perturbations in the real ISM, such as passing shock waves, or simply, general turbulent fluctuations. Small-scale entropy perturbations ( $\eta \gtrsim 1$ ), on the other hand, adhere better to the paradigm of forming near pressure-equilibrium condensations, although we have seen that a significant

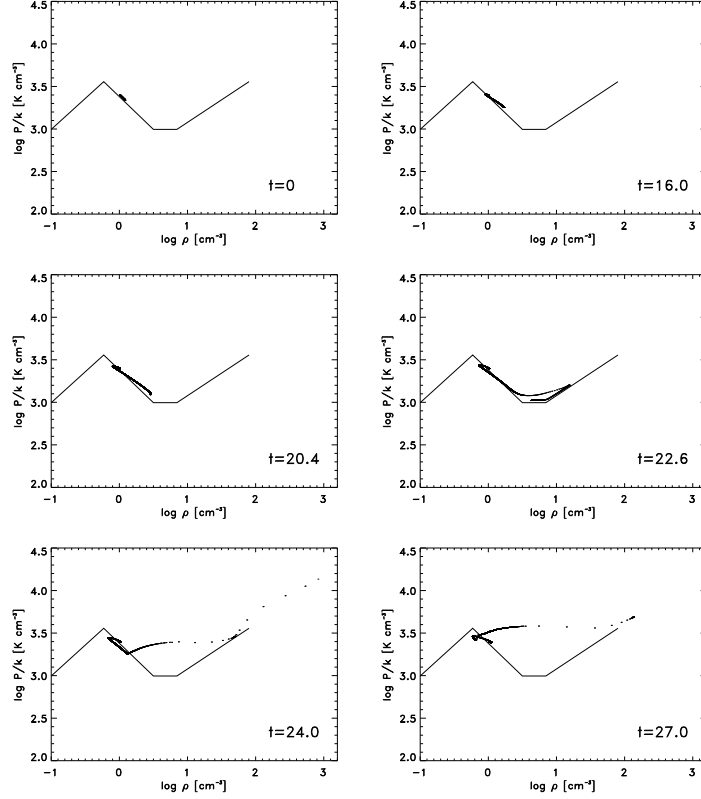


**Fig. 5.** Time development of run DEN75 in  $P$ - $\rho$  phase space. Before the shock formation, the evolution proceeds along the thermal equilibrium curve. Subsequently, the outwards-propagating shock brings the outside medium out of thermal equilibrium, and restores nearly pressure balance. Thus, the infalling gas is traversing the density “unstable” range, but in nearly isobaric (inertial) conditions, rather than along the thermal equilibrium curve.

fraction of the mass still lies in the unstable range after the cloud has formed, and is accreting onto the condensation, causing the presence of (weak) accretion fronts (rather than contact discontinuities) at the cloud boundaries that only subside asymptotically in time. Since the evacuation of the low density regions must proceed in times of order of the sound crossing time, the final fraction of mass in the “unstable” density range, in the more realistic case of multiple fluctuations, should depend on their number. In fact, we have performed simulations with a full spectrum of initial fluctuations, and in those cases the final unstable fraction may be much lower, although still times  $\gtrsim 15$  (respectively, 8) Myr are required to evacuate the unstable range when the minimum perturbation size is 12.5 (respectively, 1.25) pc. More importantly, however, entropy perturbations

may not constitute the most representative class of fluctuations present in the turbulent ISM, as we discuss in the next section.

## 5 The case of velocity fluctuations

As mentioned in §§3 and 4, velocity fluctuations are likely to be the most representative of the actual situation in the turbulent ISM, because in a continuum any density fluctuation must originate from compressive or expansive motions, thus being wavelike in nature. Such motions are readily available in a compressibly turbulent medium.

In this section we investigate the evolution of a thermally unstable medium (with respect to the isobaric criterion) subject to random forcing, as presented in Paper I. As mentioned in §3, in the case of velocity fluctuations, the dynamical time in  $\eta \equiv \tau_c/\tau_d$  is given by  $\tau_d = \min\{\tau_s, \tau_u\}$ , where  $\tau_u$  is the turbulent crossing time, which is in general also a scale-dependent quantity.

We take uniform-density initial conditions, and apply a random forcing  $f$  of the form

$$\mathbf{f}(x, t) = \hat{\mathbf{x}} \text{Re} [N \exp (ik(t)x + i\phi(t))], \quad (3)$$

where  $k(t)$  is a time dependent wavenumber,  $\phi(t)$  is the phase and  $x$  the position. Following [4], we take  $N = f_0 c_s (kc_s/\delta t)^{1/2}$ , where  $f_0$  is a constant factor and  $\delta t$  is the length of the timestep. The values of  $k/(2\pi/l)$ , where  $l$  is the box length, and of  $\phi$  are selected at each timestep randomly in the ranges  $[3, 10]$  and  $[0, 2\pi]$ , respectively. The positive exponent  $(1/2)$  in  $N$  implies that the scale of maximum forcing  $\lambda_f$  satisfies  $\lambda_f = l/10$ . A summary of the forced simulations is given in Table 1. There,  $\tau_{\text{cond}}$  is defined as the time required for a condensation to reach a density  $\rho = 10\rho_0$ ,  $\langle e \rangle$  is the ratio of the time-averaged internal energy (with the average performed over times  $0 < t < \tau_{\text{cond}}$ ) to its initial value.  $\mathcal{M}_{\text{rms}}$  is the rms Mach number, also averaged over  $\tau_{\text{cond}}$  to increase statistical confidence. Note that  $\mathcal{M}_{\text{rms}}$  fluctuates strongly in time, in contrast to  $\langle e \rangle$ , which behaves much more smoothly. The different values of  $\tau_{\text{cond}}$  in one row in Table 1 correspond to runs with different seeds for the random numbers. Table 1 shows that for simulations with box sizes 10 and 100 pc, increasing the forcing strength generally *shortens*  $\tau_{\text{cond}}$ . In the case of  $l = 100$  pc, this can be clearly understood, as the forcing scale  $\lambda_f$  is larger than  $l_{\text{eq}}$ , the scale at which  $\eta \sim 1$ , which, under the thermal rates and mean conditions of our simulations, is  $\sim 3$  pc. Thus, for  $l = 100$  pc, the forcing occurs completely in scales in which  $\eta < 1$ , and thus the wave-like fluctuations actually evolve as a condensation mode – the pressure behaves close to the thermal equilibrium curve and, rather than counteracting the turbulent compressions, enhances them. The same qualitative behavior occurs for the runs with  $l = 10$ , even though in this case  $\lambda_f \sim l_{\text{eq}}/3$ , and therefore the perturbations would have  $\eta > 1$  with respect to the unperturbed background conditions. However, in this case, the turbulent compressions are able to raise the density to large enough values that  $\eta$  effectively becomes smaller than unity within them. Thus, in this case, the triggering of condensation is essentially a nonlinear effect, analogous to that of [22].

**Table 1.** Summary of runs with forcing.

Run	$l$ [pc]	mesh points	$f_0^a$	$\langle e \rangle^b$	$\mathcal{M}_{\text{rms}}^c$	$\tau_{\text{cond}}^d$
1	3	1200	0.01	0.985	0.03	11.9, 12.1
2	3	1200	0.03	0.990	0.07	8.4, 10.85
3	3	1200	0.09	1.095	0.18	6.15, 7.8
4	3	1200	0.27	1.880	0.30	3.95, 4.6, 6.40
5	3	1200	0.36	2.450	0.30	> 16.0
6	3	2400	0.36	2.530	0.30	> 12.0
7	3	2400	0.48	3.210	0.30	> 14.0
8	3	600	0.72	3.070	0.40	> 26.0
9	3	3600	1.2	3.300	0.65	$\infty^e$
10	10	1200	0.01	0.980	0.027	10.80, 11.20
11	10	2400	0.04	0.980	0.10	7.30, 7.40
12	10	7200	0.04	0.980	0.10	7.45, 8.60
13	10	1200	0.10	0.995	0.13	5.1, 5.4, 7.0
14	10	7200	0.18	1.035	0.25	3.75, 3.90
15	10	1200	0.24	1.135	0.30	4.4, 4.6
16	10	1200	0.72	1.945	0.60	1.55, 1.70
17	100	9200	0.09	0.940	0.30	1.78, 1.90

<sup>a</sup> Forcing amplitude (cf. (3)).<sup>b</sup> Ratio of average to initial total internal energy.<sup>c</sup> rms Mach number.<sup>d</sup> Time for the first condensation to reach a density of  $10\rho_0$ .<sup>e</sup> In this case, the behavior is everywhere almost perfectly adiabatic, and it is clear that no condensations will grow.

On the other hand, Table 1 shows that in runs with  $l = 3$  pc, increasing the forcing strength first shortens  $\tau_{\text{cond}}$ , but eventually, at rms Mach numbers  $\mathcal{M}_{\text{rms}} \gtrsim 0.3$ , the condensation process is suppressed for the entire duration of the simulations. This suggests that as  $\mathcal{M}_{\text{rms}}$  increases,  $\eta$  shifts from being determined by the sound speed to being determined by the turbulent speed, while still lying in the regime  $\eta > 1$ . Note that the low value of  $\mathcal{M}_{\text{rms}}$  at which the transition from a sound- to a turbulence-dominated  $\eta$  implies that a large enough fraction of the velocity fluctuations have  $\Delta u \sim c_s$ . Thus,  $\eta \sim 3$ –10, since  $l = l_{\text{eq}}$  and  $\tau_c \approx l_{\text{eq}}/c_s$ . This estimate may be reduced somewhat because of the cooling rate increase induced by the compressions, but the suppression of the condensations suggests that in no case  $\eta$  is reduced below unity. Note also that the fact that the simulation is stabilized entirely suggests that even the time between successive

passages of shock waves through a given position in the simulation is shorter than the growth time of the perturbations.

It is interesting to note that in all cases, runs that manage to be stabilized have  $\langle e \rangle > 2$ , empirically suggesting that when the adiabatic and shock heating due to the forcing are able to at least double the internal energy of the flow with respect to the unperturbed state, the turbulent fluctuations are able to suppress the condensation process.

From the results of this section, we conclude that, for the average conditions of the ISM, the presence of turbulent motions with small enough sizes ( $\sim 0.3$  pc) and large enough amplitudes ( $\mathcal{M}_{\text{rms}} \gtrsim 0.3$ ) that  $\eta$  is maintained above unity, condensations do not appear. We understand this as a consequence of the turbulent crossing time becoming shorter than the growth time of the condensations, allowing the turbulent fluctuations to both disrupt the incipient condensations and to more than compensate cooling through the heating from shocks and adiabatic compression.

In general, we conjecture that the presence of velocity fluctuations in the ISM, even if unable to completely suppress the development of condensations, may increase the fraction of gas in the “unstable” temperature range. Note also that for small-scale velocity fluctuations, the evolution is *not* along the thermal-equilibrium curve, but rather intermediate between adiabatic and isobaric. Thus, the density range determined by the “unstable” temperature range under these conditions does not exactly coincide with the unstable density range under thermal equilibrium, as given in §3 and fig. 1. An interesting possible application for observationally measuring the actual thermodynamic state of the atomic ISM is mentioned in §8.

## 6 The magnetic pressure in turbulent media

We now make a pause in the discussion of the thermal instability and consider the character of the magnetic pressure in turbulent flows, in order to assess the possibility that it may supplement the thermal pressure in the ISM, and thus contribute to weaken the effects of TI. Note that in this section we make no attempt to discuss TI in the presence of a magnetic field. This has been discussed by a number of authors (e.g., [15,42,36,23]). Instead, here we investigate the nature of magnetic pressure in fully turbulent compressible, magnetized isothermal flows. Several works have considered this regime as well, both numerically (see, e.g., the reviews by Mac Low, Ostriker and Nordlund in this volume, and references therein), and theoretically [35]. In particular, the numerical simulations of references [44] and [43] (see also [46] for the nonisothermal case) reported a lack of correlation between the density and the magnetic pressure,  $B^2$ , where  $B$  is the magnetic field strength, at low and intermediate densities in cases in which the magnetic  $\beta$  parameter<sup>5</sup>, equal to the ratio of thermal to magnetic pressure, is  $\sim 1$ . Moreover, recent observational data (see, e.g., Crutcher, Heiles & Troland,

<sup>5</sup> The magnetic  $\beta$  should not be confused with the  $\beta_{ij}$  exponent of §§2 and 3

this volume) suggest a similar lack of correlation at densities below  $\sim 1000 \text{ cm}^{-3}$  in the ISM. Paper II has attempted to understand the origin of this decorrelation in terms of the so-called “simple” MHD waves, and discussed its implications on the role of  $B^2$  as a pressure. In this section we briefly summarize the results of that paper.

We consider isothermal MHD flows in “1+2/3” dimensions, or slab geometry (cf. §2). The direction  $x$  is referred to as the direction of wave propagation. In this setup,  $b_x$ , the field component along  $x$ , is constant. We denote by  $b$  the magnitude of the field component perpendicular to  $x$ . The initial, uniform magnetic field is chosen to lie in the  $(x, z)$  plane, at an angle  $\theta$  from the  $x$  axis, so that  $b_x = \cos \theta$  at all times. The parameters characterizing the flow are the sonic and Alfvénic Mach numbers of the non-dimensional velocity unit, denoted  $M_s$  and  $M_A$ , respectively, and the propagation angle  $\theta$ . The plasma beta is then  $\beta = M_A^2/M_s^2$ .

“Simple” MHD waves (see, e.g., [33,37]) are finite-amplitude solutions of the equations, characterized by the property that all variables can be expressed as wave “profiles”, i.e., as a function of a single one of them (say, the density) as in the case of linear MHD waves. The same well known modes of the linear case, i.e., Alfvén, fast, and slow, exist in the case of simple waves. Only the latter two are associated with the density fluctuations. The propagation velocities of the

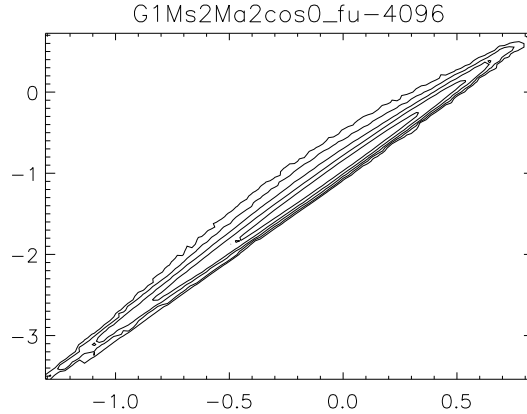


**Fig. 6.** Magnetic pressure-density correlation, indicated by the two-dimensional histogram of points in log-log coordinates, for a simulation with a magnetic field perpendicular to the direction of propagation (i.e.,  $\cos \theta = 0$ ), and forcing parallel to this direction. This configuration allows only the existence of the fast mode of nonlinear MHD waves. The run has an rms field fluctuation  $\delta B/B = 0.6$ . The rms Alfvénic Mach number  $M_{A \text{ rms}}$  (not to be confused with the parameter  $M_A$ ) is undefined in this purely magnetosonic case. The magnetic pressure is seen to scale as  $\rho^2$ .

modes are given by [33,37]

$$v_{\pm}^2 = \frac{1}{2M_a^2\rho} (B^2 + \beta\rho) \left( 1 \pm \sqrt{1 - \frac{4\beta b_x^2\rho}{(B^2 + \beta\rho)^2}} \right) \quad (4)$$

and

$$v_A = \pm \frac{b_x}{M_a\rho^{1/2}}, \quad (5)$$

where  $v_{\pm}$  denotes the speed of the fast (+) and slow (−) modes, and  $v_A$ , that of the Alfvén mode.  $B^2 = b_x^2 + b^2$  is the total field strength.

After manipulating the equations to obtain the wave profiles, one finds, in particular, for the dependence of the field with density,

$$\frac{d}{d\rho} \frac{b^2}{2} = \frac{d}{d\rho} \frac{B^2}{2} = (M_a^2 v^2 - \beta). \quad (6)$$

In the limit when  $4\beta b_x^2\rho \ll (B^2 + \beta\rho)^2$ , this equation can be simplified and integrated using (4) to give the dependences for the fast and slow modes as

$$\frac{b^2}{b_x^2} \approx C - 2\frac{\beta\rho}{b_x^2} \quad (\text{slow mode}) \quad (7)$$

$$\frac{b^2}{b_x^2} \approx \frac{\rho^2}{b_x^2} - 1 \quad (\text{fast mode}), \quad (8)$$

where  $C$  is a constant. These equations essentially give the behavior of magnetic pressure with density for the two modes in the limit mentioned above. This condition is generally satisfied, except when  $\beta\rho \approx b_x^2$  and simultaneously  $b^2 \ll b_x^2$ , i.e., when  $b_x$  is not too small, for  $\beta$  of order unity and small field distortions.

Several points are noteworthy about (7) and (8): 1) The  $\beta$  weighting in the second term of the RHS of (7) implies that at low  $\beta$ , the slow mode produces large density fluctuations even when the field fluctuations are small. 2) The total pressure,  $P_{tot} = \frac{b^2}{2M_A^2} + \frac{\rho}{M_s^2}$ , is roughly constant in the slow mode. 3) Most importantly, the pressures from the two modes depend very differently on density. One can then expect that, in the large fluctuation amplitude case (i.e., the fully nonlinear regime), *the particular value of the magnetic pressure of a fluid parcel will not be uniquely determined by its density, but instead, that it will depend on the detailed history of how the density fluctuation was arrived at*, causing a lack of correlation between the magnetic pressure and the density.

The latter suggestions have been tested in Paper II by means of numerical simulations with random forcing (actually, an acceleration) applied on wavenumbers 1-19 to all three velocity components or to only the perpendicular ones. Choosing the direction of the forcing and of the uniform magnetic field allows us to highlight either one of the slow and fast modes. Figure 6 shows the  $b^2$ - $\rho$  correlation by means of isocontours of the two-dimensional histogram in the  $\log(b^2/2M_A^2)$ - $\log(\rho)$  plane of the points in a simulation with 4096 grid points, forcing applied on all three velocity components, and the initial magnetic field



perpendicular to the direction of propagation, at intermediate Alfvénic Mach number ( $M_A = 2$ ). This is a case in which only the fast mode exists, consisting of a pure magnetosonic wave, and the correlation exhibits the well known  $\rho^2$  behavior of magnetic pressure in this case.

Figure 7, on the other hand, shows the correlation for a run at the same resolution with the forcing perpendicular to the propagation direction, and the magnetic field almost parallel to the forcing ( $b_x = \cos\theta = 0.1$ ), at low Alfvénic Mach number ( $M_A = 0.15$ ). In this case, the density fluctuation production is dominated by the slow mode because  $\langle\beta\rangle \sim 0.007$  (c.f. (7)). The near constancy of the total pressure in this case is evident in this figure. In this simulation, one observes large oscillating density clumps which do not merge nor pass each other. However, for this same field configuration, as  $M_A$  is increased, the field becomes more strongly distorted, and the fast mode starts acting on the perturbed field. The fluctuations become more random and superpose each other. The result is that at high  $M_A$  both modes are actively producing density fluctuations, and the correlation between magnetic pressure and the density is lost, as seen in fig. 8. The situation can be idealized by assuming that the density of each fluid parcel is arrived at through a random sequence of slow and fast waves, which is different for each parcel.

The case of parallel propagation is also interesting to mention as it illustrates the complexity of this problem. For example, the picture of non-interacting clumps observed at small  $M_A$  (i.e. in presence of weak field distortions) and for large angles is also observed for parallel propagation in the case of large  $M_A$ . But in that case the clumps form inside strong slow shocks. The magnetic field

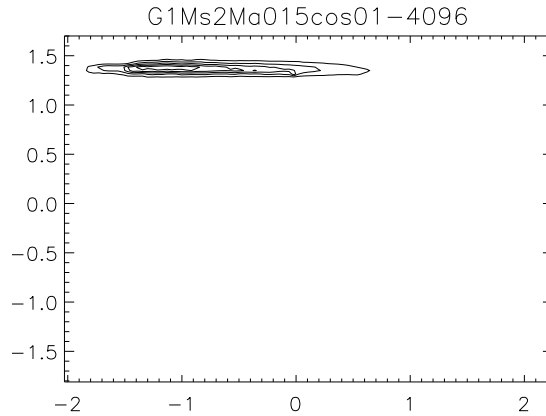


**Fig. 7.** Magnetic pressure-density correlation for a simulation with  $\cos\theta = 0.1$ , and forcing perpendicular to the propagation direction, with  $\delta B/B = 0.31$  and  $M_{A \text{ rms}} = 4.85$ . This configuration highlights the slow mode. The magnetic pressure is seen to remain virtually constant.

intensity is the weakest inside the clumps which cannot merge due to the high external magnetic pressure. In the general 3D case, we expect all angles between the magnetic field and the propagation direction to be present, and therefore a representative case would be one in which the field is at  $45^\circ$  from the propagation direction. In this case, we recover the trend of a roughly constant magnetic pressure at small  $M_A$  and an increased scatter between the magnetic pressure and density as  $M_A$  is increased (not shown).

We conclude from this section that the scatter between magnetic pressure and density found in simulations and in observational data can be understood in terms of the different dependence of the magnetic intensity on density for the slow and fast modes of simple nonlinear MHD waves, and of the random sequence of these that a fluid parcel experiences as it evolves in a fully turbulent regime. Moreover, a number of important implications emerge from this lack of correlation. First, it suggests that modeling magnetic pressure by means of a polytropic dependence on density may not be adequate in the fully turbulent case. Second, the magnetic “pressure” does not really act as a pressure, as it does not behave as a restoring force in general. Instead, it acts more as a random forcing. Third, the latter point suggests that magnetic pressure should not be effective as a substitute for thermal pressure when the latter behaves “in reverse” in thermally unstable situations. A final note is that the isothermality of the flows considered here is of no relevance to the results, which are thus expected to apply equally to non-isothermal flows.

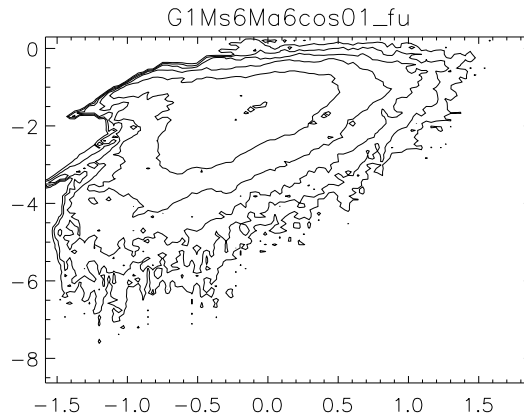


**Fig. 8.** Magnetic pressure-density correlation for a simulation with  $\cos \theta = 0.1$ , and forcing in the three directions. This configuration also highlights the slow mode, but increases the field distortions ( $\delta B/B = 1.75$  and  $M_{A\text{rms}} = 56$ ). The magnetic pressure is seen to decorrelate from the density, although it appears to be bounded above and below by the slow and fast mode dependences, respectively.

## 7 TI in models of the ISM

### 7.1 Mass fraction in the unstable range

In the previous sections we have discussed the nonlinear development of fluctuations of various kinds and sizes in the presence of TI under the isobaric criterion, and the nature of magnetic pressure in turbulent media. With this background we can now proceed to discuss the behavior of numerical models of the ISM incorporating the magnetic field, self-gravity, rotation, shear, and stellar-like (localized) energy injection, in the presence of isobaric TI. These have been presented in Papers III and IV, but here we present some further discussion of their results in the light of the previous sections.

As mentioned in the introduction, the classic two- and three-phase models of the ISM were based on the principles of thermal and pressure equilibrium, and thus did not predict the existence of significant amounts of gas in-between the phases. Yet, observations do not clearly confirm this, and instead often have found evidence of significant amounts of “lukewarm” gas at temperatures intermediate between those of the cold and warm phases [10,26,52,17,21]. Thus, it is important to perform numerical simulations that quantify this fraction and that allow us to determine whether sharp phase segregation is expected in the ISM, or whether it is more likely a continuum. In fact, previous simulations, although not specifically aimed at this issue, had already pointed towards the existence of unstable gas as well [20,29].

In Papers III and IV, the probability distribution functions (PDFs) of density and temperature were studied in 2D numerical simulations of the ISM including all the agents mentioned above at large scales, with a box size of 1 kpc, on the Galactic plane. The magnetic field has a uniform component of  $1.5 \mu\text{G}$  on the  $x$ -direction, and an initial rms fluctuation amplitude of  $4.5 \mu\text{G}$ . The energy injection mechanism consists of small-scale ( $\sim 10$  pixels across) heat sources turned on at sites where the density exceeded a certain threshold (within the cold stable branch of the density range), that remain on for 6 Myr, mimicking the effect of ionization heating from OB stars in HII regions. Paper III used a rather low resolution ( $128^2$  grid points), so that, in effect, only large scales such as those considered in run DEN75 of §4 were resolved. In this case, the density PDF for thermally unstable cases (fig. 9) was found to be virtually identical as that for thermally stable cases, with no noticeable gap in the unstable density range, implying that no sharp transition between the cold and warm phases existed.<sup>6</sup> Note that other simulations we performed, using large-scale random forcing and considering only a thermally unstable flow without the other physical ingredients, did produce bimodal density distributions. This is because, with respect to the large-scale forcing, the flow responds along the thermal equilibrium curve, and presents no resistance to compression in the unstable density range.

<sup>6</sup> Note that, for the combined case with magnetic fields, self-gravity and rotation, the instability criterion is actually different [11,14,46]. The simulations were ensured to be unstable under the combined criterion as well.

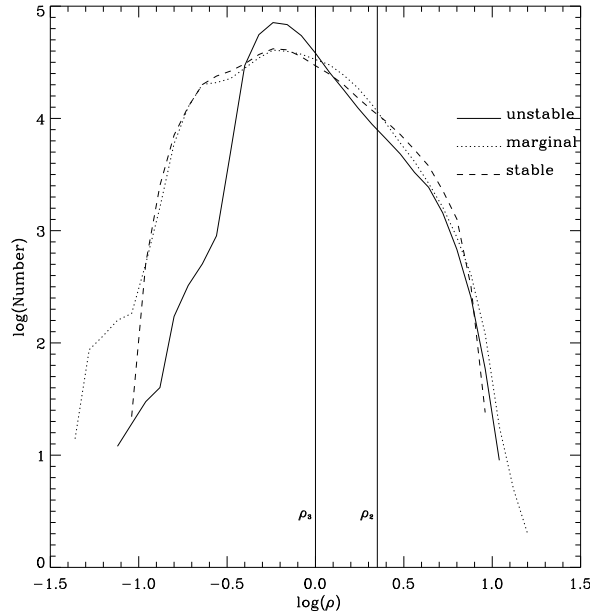


**Fig. 9.** Density PDFs for three ISM simulations from Paper III of a 1-kpc region on the Galactic disk at low resolution ( $128^2$ ), including the magnetic field, the Coriolis force, self-gravity, and stellar-like energy injection, consisting of small-scale heat sources placed at sites of high density. The cooling functions used imply either stability, marginal stability ( $\gamma_{\text{eff}} = 0$ ), or instability with respect to the isobaric criterion. The PDF is seen to be virtually insensitive to the presence of the instability.

Paper IV then examined, at larger resolution ( $512^2$  grid points), the PDFs of the temperature field. The temperature PDFs were indeed found to be bimodal, with peaks at the temperatures of the warm and cold phases, but still containing  $\sim 50\%$  of the mass in the unstable temperature range (fig. 10). Moreover, images of the temperature field show that the gas at temperatures in the unstable range occupies a sizeable fraction of the volume (fig. 11).

Some caveats concerning Papers III and IV should be mentioned, however. First, there is the concern that the box size considered, and the resolutions used, especially in Paper III, did not resolve the fastest-growing small scales, which would be the ones most prone to cause fragmentation in the unstable range. Moreover, the shear used had a sinusoidal rather than monotonic profile for numerical reasons [46]. According to the combined stability criterion for the 2D case [46], the shear is stabilizing when it has a sign opposite to that of the actual Galactic disk. Half of the simulation box presented in Paper IV had such a sign of the shear. Thus, we have subsequently performed an additional simulation with the same resolution ( $512^2$ ) as the main one of Paper IV, but without shear and with a box size of 150 pc, thus effectively resolving scales down to a few

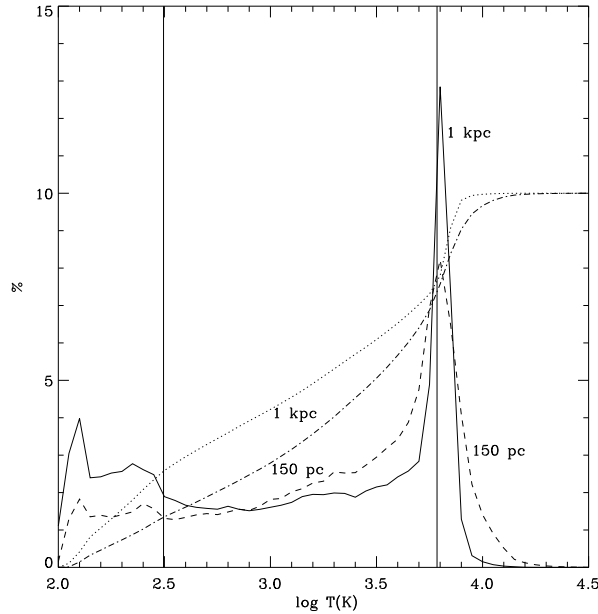


**Fig. 10.** Mass-weighted temperature PDF (solid line) and cumulative distribution (dotted line) for a simulation from Paper IV, similar to those from Paper III but using a fit to the standard cooling function from [56], and higher resolution ( $512^2$ ). Also shown are the PDF (dashed line) and cumulative distribution (dot-dashed line) for a simulation at the same resolution for a 150-pc box, and without differential rotation shear. Roughly 50% of the mass is in the “unstable” temperature range in both simulations. The two simulations are shown at the same physical time (52 Myr).

parsecs (taking into account the effects of artificial diffusivity). This simulation gives similar results as those from Paper IV, and in fact gives a somewhat larger fraction of mass in the unstable range, at the expense of mass in the cold phase (fig. 10).

Nevertheless, simulations at even larger resolutions, or with smaller box sizes, are still desirable. In this regard, it is worth noting that reference [32] has performed simulations of turbulence generation by the pure nonlinear development of TI in 3D with box sizes down to 6 pc and resolution  $256^3$ , and still finds 15–25% of the mass in the unstable range. All numerical evidence thus points toward the existence of a sizeable mass fraction in the unstable range when the flow is in a turbulent state.

## 7.2 Discussion

The reason why there appear to be such large quantities of gas in the unstable regime is an important question. In this paper we have outlined at least two

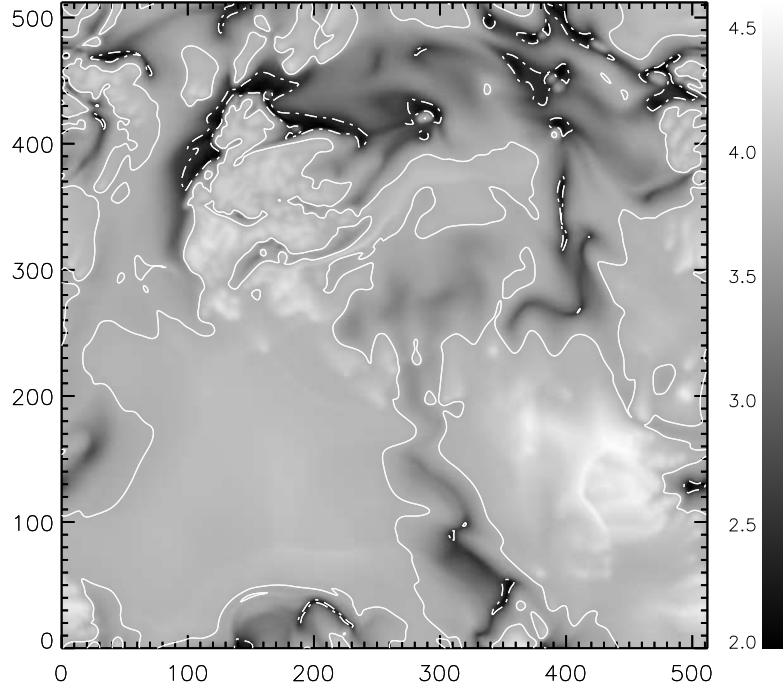


**Fig. 11.** Temperature field of the 150-pc simulation of the ISM whose histogram is shown in fig. 10. The resolution is  $512^2$  grid points. The (logarithmic) temperature scale is shown in the bar at the right. The highest temperatures correspond to regions of “star formation” clustering, in which the heating from many stars combines additively. The contours mark the upper (solid lines) and lower (dash-dotted line) boundaries of the unstable temperature range, showing the large fraction of the volume occupied by gas in this range, and the smooth transition between this range and higher and lower temperatures.

possible mechanisms. One, encountered in §4, is simply that, for entropy perturbations starting from unstable conditions, a substantial fraction of the gas in the simulation still remains in the “unstable” range by the time the condensation process is completed, because *the evacuation occurs roughly on the sound crossing time for the large voids* that are generated. Thus, the evacuation of the unstable range can take much longer times than the formation of the condensations, especially small-scale ones (if the spatial density of perturbations is not too large), and in the meantime the gas being evacuated remains in the unstable range. Moreover, this gas is not truly unstable, because, rather than evolving along the thermal equilibrium curve, it does so along nearly isobaric conditions, with the same sign of the density and pressure gradients everywhere. This is because this is precisely the flow *resulting* from the instability, after a pressure-equalizing front has propagated outwards from the formed cloud.

The second mechanism is that, in a turbulent medium, the density fluctuations have their origin in compressive motions, which can more than compensate the cooling through the adiabatic and shock heating. In §5 we have shown that, for initial conditions with the mean density of the ISM and its corresponding thermal-equilibrium temperature ( $\rho \sim 1 \text{ cm}^{-3}$ ,  $T \sim 2500 \text{ K}$ ), velocity fluctuations at scales  $\sim 0.3 \text{ pc}$  and with rms Mach numbers  $\sim 0.3$  do not undergo any sort of condensation for arbitrarily long times. This level of fluctuations at such scales is not unrealistic. Although this cannot be the explanation for the unstable mass fraction observed in the simulations of Papers III and IV, because these scales were not resolved there, it is probably a contributing mechanism to maintaining gas in the “unstable” range in the ISM.

It should be pointed out that reference [32] proposes that, in its 3D simulations of turbulence generation by the pure nonlinear development of TI, the presence of unstable gas is due to “turbulent diffusion”. This requires that the turbulent crossing time of the fluctuations be shorter than the cooling time within them, and thus corresponds to our requirement of  $\eta > 1$  for velocity fluctuations. However, it is noteworthy that in their simulations, the turbulence is induced by the development of TI itself, thus suggesting that the nonlinear advection term has managed to “lose memory” of the initial conditions, so that apparently even the turbulence generated by TI itself can end up providing velocity fluctuations which are not directly following the reversed pressure gradient from it.

Finally, from the results of §6, we conclude that the magnetic field is probably not a dominant effect in maintaining the population of unstable gas in the sense of providing a supplemental pressure counteracting the reversed thermal pressure from TI. However, its behavior as a random forcing may have the same stabilizing effect as the random force we have used in §5.

## 8 Summary and conclusions

In this paper we have summarized the results from various studies aiming at understanding the role of TI in the turbulent atomic ISM, and the behavior of the

magnetic pressure in the fully turbulent case. The motivation has been twofold. On the one hand, the classic multi-phase models of the ISM have neglected the implications of the ISM being turbulent, and it is thus important to assess the consequences of the presence of turbulence on the thermal and spatial structure of this medium. On the other hand, observations have often suggested the presence of gas with temperatures in the thermally unstable range, in apparent contradiction with the multi-phase models.

We first considered the nonlinear stages of evolution of entropy perturbations, in order to quantify the magnitude of the speeds developed and the times required for completing the condensation process as a function of the parameter  $\eta$ , the ratio of the cooling time to the dynamical crossing time. We found that large-scale initial perturbations ( $\gtrsim 15$  pc,  $\eta \lesssim 0.2$ ) develop supersonic speeds, require times  $\gtrsim 10$  Myr to complete the condensation process, and end up with densities and pressures above the thermal equilibrium value due to the ram pressure of the still infalling gas. Those times are long compared with typical times between successive external shock passages, and star formation time scales. We thus concluded that clouds formed from perturbations of such sizes (although the resulting cloud has a size  $\sim 1$  pc) are unlikely to exist in thermal pressure equilibrium with their surroundings. Initial perturbations of sizes  $\sim 3$  pc, on the other hand, require times  $\sim 4$  Myr to complete their evolution and do not generate supersonic speeds, thus reaching a more quiescent final state, and adhering better to the paradigm of thermal-pressure bounded clouds, although, by the time the cloud has formed, accretion is still occurring, so that the clouds are bounded by weak accretion fronts, rather than contact discontinuities. Furthermore, the gas still accreting is necessarily in the unstable temperature range, although it is not in thermal equilibrium, but rather it has a “normal” pressure behavior ( $P$  increases with  $\rho$ ), and thus it is not prone to further fragmentation.

More importantly, we then studied cases subject to random forcing, finding that precisely small-scale ( $\sim 0.3$  pc) *velocity* fluctuations of moderate Mach numbers are capable of suppressing the growth of condensations at scales  $\lesssim 3$  pc. So, even though pure entropy perturbations at small scales are the best candidates for forming thermal-pressure bounded clouds, they are also the easiest to prevent from growing by velocity fluctuations. Thus we conclude that the scenario of thermal-pressure bounded clouds is unlikely in general in a medium subject to external sources of turbulence.

We then considered the magnetic field as an additional source of pressure in the ISM, confirming earlier results that at low and intermediate densities the magnetic pressure is strongly decorrelated from density in fully turbulent cases (large field fluctuations), and proposed an interpretation of this phenomenon in terms of the scaling of  $B^2$  with density for the slow and fast modes of simple nonlinear MHD waves. The decorrelation between magnetic pressure and density has several implications, among which is that the magnetic field probably is ineffective in supplementing thermal pressure in thermally unstable conditions, and that it is probably inadequate to model magnetic pressure by means of an equivalent polytropic behavior in the fully turbulent case.



Finally, we considered simulations of the full ISM at large and intermediate scales and at various resolutions, finding in all cases that a significant fraction of the mass dwells in the unstable temperature regime. In the light of the previous results, this appears to be not a consequence of the additional pressure supplied by the magnetic field, but of the fact that reaching the warm diffuse phase takes longer times than producing condensations, because the time involved is the crossing time of the large voids produced, and that velocity perturbations at small scales ( $\eta > 1$ ) can suppress or delay the condensation process.

A final remark of interest is that it may be possible to determine observationally whether the gas seen at unstable temperatures corresponds to the out-of-thermal-equilibrium gas observed in the simulations by either a) simultaneously determining two of its thermodynamic variables, or b) comparing directly observed cooling rates (e.g., fine structure lines) with theoretical estimates of the heating rate (e.g., photoelectric heating) in specific regions. If this is confirmed, then it would provide strong evidence that turbulent motions populate all regions of the thermodynamic variable space, preventing a sharp segregation of the atomic ISM into the stable phases of TI.

It is a pleasure to acknowledge stimulating exchanges with C. Heiles, P. Hennebelle, J. Scalo and E. Zweibel. This work has received partial financial support from CONACYT grant 27752-E, from the French national program PCMI and from the conference organizers to E.V.-S., and has made use of NASA's Astrophysics Data System Abstract Service.

## References

1. S.A. Balbus: 'Thermal Instability'. In: *The Physics of the Interstellar Medium and Intergalactic Medium*, ed. by A. Ferrara, C.F. McKee, C. Heiles, P.R. Shapiro (Astronomical Society of the Pacific, San Francisco 1995), p. 328
2. J. Ballesteros-Paredes, E. Vázquez-Semadeni, J. Scalo: *ApJ* **515**, 286 (1999)
3. M.C. Begelman, C.F. McKee: *ApJ* **338**, 375 (1990)
4. A. Brandenburg: *ApJ* **550**, 824 (2001)
5. W. Brinkmann, S. Massaglia, E. Müller: *Astron. Ap.* **237**, 536 (1999)
6. A. Burkert, D.N.C. Lin: *ApJ* **537**, 270 (2000)
7. W.-H. Chiang, J.N. Bregman: *ApJ* **328**, 427 (1988)
8. A. Dalgarno, R.A. McCray: *Ann. Rev. Astron. Ap.* **10**, 375 (1972)
9. L.P. David, J.N. Bregman, C.G. Seab: *ApJ* **329**, 66 (1988)
10. J.M. Dickey, E.E. Salpeter, Y. Terzian: *ApJ* **211**, L77 (1977)
11. B.G. Elmegreen: *ApJ* **378**, 139 (1991)
12. B.G. Elmegreen: 'The Origin and Evolution of Giant Molecular Clouds'. In: *The Physics of Star Formation and Early Stellar Evolution*, ed. by C.J. Lada, N.D. Kylafis (Kluwer, Dordrecht, 1991), p. 35
13. B.G. Elmegreen: *ApJ* **419**, L29 (1993)
14. B.G. Elmegreen: *ApJ* **433**, 39 (1994)
15. G.B. Field: *ApJ* **142**, 531 (1965)
16. G.B. Field, D.W. Goldsmith, H.J. Habing: *ApJ* **155**, L149 (1969)
17. E.L. Fitzpatrick, L. Spitzer: *ApJ*, **475**, 623 (1997)

18. A. Gazol, E. Vázquez-Semadeni, F.J. Sánchez-Salcedo, J. Scalo: ApJ **557**, 121 (2001) (Paper IV)
19. H. Gerola, M. Kafatos, R. McCray, R.: ApJ **189**, 55 (1974)
20. J.P.E. Gerritsen, V. Icke: Astron. Ap. **325**, 972 (1997)
21. C. Heiles: ApJ **551**, L105 (2001)
22. P. Hennebelle, M. Pérault: Astron. Ap. **351**, 309 (1999)
23. P. Hennebelle, M. Pérault: Astron. Ap. **359**, 1124 (2000)
24. J.H. Hunter: ApJ **161**, 451 (1970)
25. J.H. Hunter: ApJ **166**, 453 (1971)
26. P.M.W. Kalberla, U.J. Schwarz, W. M. Goss: Astron. Ap. **144**, 27 (1985)
27. H. Kang, G. Lake, D. Ryu: J. Kor. Astron. Soc. **33**, 111 2000
28. P. Kornreich, J. Scalo: ApJ **531**, 366 (2000)
29. M.J. Korpi, A. Brandenburg, A. Shukurov, I. Tuominen, ÅNordlund: ApJ **514**, L99 (1999)
30. H. Koyama, S.-I. Inutsuka: ApJ **532**, 980 (2000)
31. H. Koyama, S.-I. Inutsuka: astro-ph/0112420 (2001)
32. A. Kritsuk, M.L. Norman: astro-ph/0112437 (2001)
33. L.D. Landau, E.M. Lifshitz: *Fluid Mechanics*, 2nd edn. (Pergamon Press, Oxford, 1987)
34. A. Lioure, J.-P. Chièze: Astron. Ap. **235**, 379 (1990)
35. Y. Lithwick, P. Goldreich: ApJ **562**, 279 (2001)
36. M. Loewenstein: ApJ **349**, 471 (1990)
37. G. Mann: J. Plasma Phys. **53**, 109 (1995)
38. C.F. McKee, J.P. Ostriker: ApJ **218**, 148 (1977)
39. B. Meerson: Rev. Mod. Phys. **68**, 215 (1996)
40. S.D. Murray, D.N.C. Lin: ApJ **339**, 933 (1989)
41. S.D. Murray, D.N.C. Lin: ApJ **363**, 50 (1990)
42. E.E. Oran, J.T. Mariska, J.P. Boris: ApJ **254**, 349 (1982)
43. E.C. Ostriker, J.M. Stone, C.F. Gammie: ApJ **546**, 980 (2001)
44. P. Padoan, Å Nordlund: ApJ **526**, 279 (1999)
45. A. Parravano: ApJ **172**, 280 (1987)
46. T. Passot, E. Vázquez-Semadeni, A. Pouquet: ApJ **455**, 536 (1995)
47. T. Passot, E. Vázquez-Semadeni: in preparation (2002) (Paper II)
48. F.J. Sánchez-Salcedo, A. Brandenburg: Mon. Not. Royal Astron. Soc. **322**, 67 (2001)
49. F.J. Sánchez-Salcedo, E. Vázquez-Semadeni, A. Gazol: ApJ submitted (2002) (Paper I)
50. J. Schwarz, R. McCray, R.F. Stein: ApJ **175**, 673 (1972)
51. F.H. Shu: *The Physics of Astrophysics. Vol. II: Gas Dynamics*, (University Science Books, Sausalito, 1992)
52. L. Spitzer, E.L. Fitzpatrick: ApJ **445**, 196 (1995)
53. E. Vázquez-Semadeni, T. Passot, A. Pouquet: ApJ **473**, 881 (1996)
54. E. Vázquez-Semadeni, A. Gazol, J. Scalo: ApJ **540**, 271 (2000) (Paper III)
55. K. Wada, M. Spaans, S. Kim: ApJ **540**, 797 (2000)
56. M.G. Wolfire, D. Hollenbach, C.F. McKee, A.G.G.M. Tielens, E.L.O. Bakes: ApJ **443**, 152 (1995)